East European Journal of Physics. **3.** 286-297 (2025)
DOI:10.26565/2312-4334-2025-3-26 ISSN 2312-4334

EFFECT OF COBALT DOPING ON THE STRUCTURAL, MORPHOLOGICAL, OPTICAL, AND MAGNETIC PROPERTIES OF ZnO THIN FILMS PREPARED BY ULTRASONIC SPRAY TECHNIQUE

Z. Daas[a], A. Bouabellou[a], K. Daas[b], D. Belfennache[c]*, K. Benzouai[a], M. Mahtali[a], R. Yekhlef[c]
[a]*Thin Films and Interfaces Laboratory, Constantine 1- Frères Mentouri University, 25017 Constantine, Algeria*
[b]*Laboratory of Mathematics and Their Interactions, Boussouf Abdelhafid University Center, Mila, Algeria*
[c]*Research Center in Industrial Technologies CRTI, P.O. Box 64, Cheraga, 16014 Algiers, Algeria*
**Corresponding Author E-mail: belfennachedjamel@gmail.com*
Received June 1, 2025; revised July 29, 2025; accepted August 5, 2025

Zinc-cobalt oxide ($Zn_{1-x}Co_xO$) thin films refer to a semiconductor material based on zinc oxide (ZnO) doped with cobalt (Co). This material is studied mainly for its modified magnetic, electronic and optical properties, particularly in the context of diluted magnetic semiconductors (DMS). This study analyzes the effect of cobalt doping on the structural optical, and magnetic properties of ZnO thin films, fabricated using alow-cost, scalable ultrasonic spray technique. Zinc-cobalt oxide ($Zn_{1-x}Co_xO$) thin films were successfully deposited on glass substrates using the ultrasonic spray pyrolysis technique at a substrate tem- perature of 450 ◦C, with cobalt doping concentrations of x = 0%, 1%, 3%, and 5%. X-ray diffraction (XRD) analysis revealed a hexagonal wurtzite structure for all samples, with no secondary phases, indicating effective incorporation of Co^{2+} ions into the ZnO lattice. Raman spectroscopy indicated the emergence of structural disorder and defect-related modes, consistent with the increase in Urbach energy. Scanning electron microscopy (SEM) showed granular surface morphologies, and a non-homogeneous surface pattern is visible on all samples. Atomic Force Microscopy (AFM) showed an increase in surface roughness and grain size with increasing doping concentration. Optical measurements confirmed high transmittance in the visible range and a gradual de- crease in optical band gap from 3.21 eV to 2.95 eV with increasing Co content. The spectroscopy, and vibrating sample magnetometer (VSM) revealed that all films are intrinsically ferromagnetic. The origin of the ferromagnetism was found to be an intrinsic property of the Co-doped ZnO thin films.
Keywords: *Spray Technique, ZnO Thin Films, Cobalt doping, RAMAN, Diluted Magnetic Semiconductors (DMS)*
PACS: 73.50.-h, 73.50.Pz

1. INTRODUCTION

Semiconductors play a fundamental role in modern technology due to their ability to control the flow of electricity, thus enabling the manufacture of components such as transistors and integrated circuits that are the basis of computers, smartphones and other electronic devices [1,2]. They are also used in solar panels for the conversion of solar energy into electricity [3-5]. Zinc oxide (ZnO) is one of the most competitive transparent semiconductors. It can crystallize under normal conditions of temperature and pressure in the wurtzite structure which is the most stable and preferred [6,7]. This structure formed by the stacking of planes of atoms (O^{2-}) and (Zn^{2+}) in tetrahedral coordinates does not have a center of symmetry, which generates a spontaneous polarization field along the c axis [8]. This polarity as well as the piezoelectric polarity thermodynamically favor the preferential growth of ZnO along the (002) direction and improve their mechanical and optoelectronic properties [9]. In recent years, many researchers have discovered some extraordinary elements with better chemical, electronic, optical and especially magnetic qualities [10,11]. Doping is the most commonly used strategy to improve the quality of semiconductors [12,13]. Due to the excellent characteristics (optical, electrical and magnetic) of transition metals, especially cobalt, Co-doped ZnO ($Zn_{1-x}Co_xO$) thin films are widely used in industry for applications such as optoelectronics, spintronics, sensors, …etc. [14,15].

Several methods have been used to synthesize thin films, including: Sol-gel processes [16], metal-organic chemical vapor deposition (MOCVD) [17], Micro-ondes-Cyclotron Résonance Électronique (MW-ECR) [18], Plasma-Enhanced Chemical Vapor Deposition (PECVD) [19] chemical bath deposition (CBD) [20], sputtering [21], and spray technique [22]. The latter is one of the most used techniques among them, because of the potent technique for creating a variety of powdered materials, including metals, metal oxides, superconducting materials, and nanophase materials, is spray pyrolysis. It also offers several advantages over alternative powder synthesis methods, including superior control over chemical uniformity, stoichiometry in multi-component systems, and high powder purity.

It should be remembered that cobalt is clearly capable of modifying the various properties of ZnO. Indeed, much research has been done to study the effect of cobalt doping on the optical, structural, and morphological properties of ZnO thin films. However, little effort has been devoted to explaining the effect of cobalt doping on the ferromagnetic properties of the ZnO thin films. Our work consists in developing thin films of $Zn_{1-x}Co_xO$, deposited on glass substrates by spray technique. Our objective is to consider a correlation between the Co doping effect and the structural, morphological, optical and magnetic properties of the thin films obtained. To achieve this objective, the structure, morphology as well as the optical and magnetic properties of the layers produced were studied using different techniques: X-ray diffraction

---

Cite as: Z. Daas, A. Bouabellou, K. Daas, D. Belfennache, K. Benzouai, M. Mahtali, R. Yekhlef, East Eur. J. Phys. 3, 286 (2025), https://doi.org/10.26565/2312-4334-2025-3-26

(XRD) and Raman spectroscopy, scanning electron microscopy and atomic force microscopy (SEM and AFM), UV-Visible, the spectrophotometry, spectroscopy, and vibrating sample magnetometer (VSM).

2. EXPREMENTAL PROCEDURE

Spray ultrasonics was used to deposit the $Zn_{1-x}Co_xO$ thin films (where x = 0, 0.01, 0.03, and 0.05) on glass substrates. Precursors included cobalt acetate tetrahydrate $[Co(CH_3COO)_2{\cdot}4H_2O]$ and zinc acetate dihydrate $[Zn(CH_3COO)_2{\cdot}2H_2O]$. The spray solution was made by dissolving the powders in methanol at the appropriate molar ratios, keeping the molarity at 0.1 mol L^{-1}. An ultrasonic nebuliser, which transforms liquid into a consistent stream of small droplets with an average diameter of 40 µm (as defined by the manufacturer), was then used to spray the solution onto heated glass substrates. The thin films were deposited for 2 min at a temperature of 450 ◦C.

3. RESULTS AND DISCUSSION

3.1 The XRD Analysis of Co-doped ZnO Thin Films

The X-ray diffraction (XRD) patterns of Co-doped ZnO thin films at different doping concentrations (0%, 1%, 3%, and 5%) are presented in Fig. (1.a).

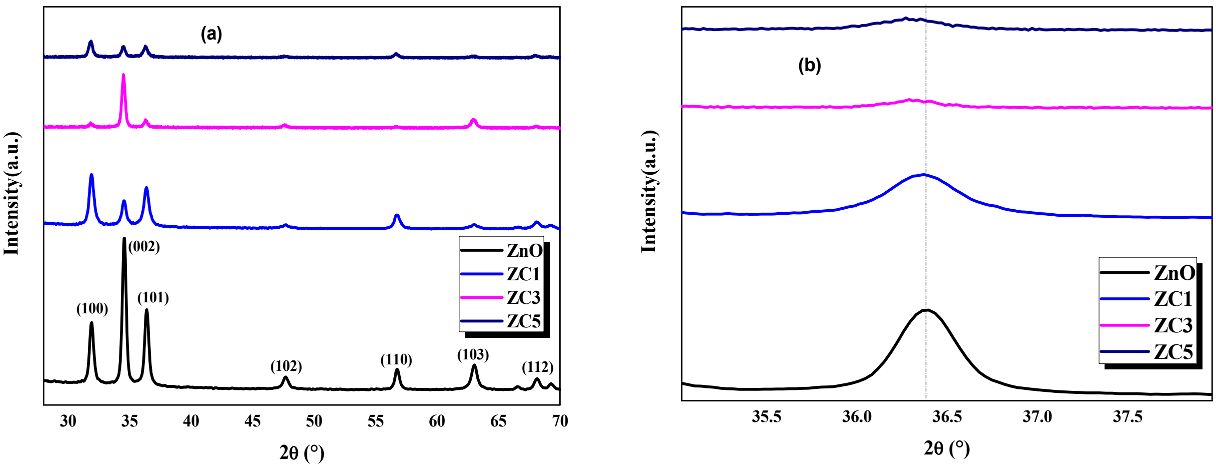

Figure 1. X-ray diffraction spectra of ZnO thin films doped with cobalt at different concentrations, (a) XRD pattern, (b) Zoomed-in view of the (101) diffraction peak

The diffraction peaks appear at 2θ = 31.92◦, 34.56◦, 36.39◦, 47.62◦, 56.72◦, 62.95◦, 67.97◦, and 69.19◦ corresponding to the (100), (002), (101) ,(102), (110),(103), (112), and (201) crystallographic planes, respectively, in the undoped ZnO sample. This confirms that the samples possess a hexagonal wurtzite structure and belong to the space group P 63mc, as reported in JCPDS card No. 36–1451 [23]. Fig. (1.b) shows an enlarged view of the (101) peak, where a slight shift in the peak position is observed compared to pure ZnO, indicating the successful incorporation of Co^{2+} ions into the ZnO crystal lattice [24]. Furthermore, no secondary phases or structural changes are detected due to Co doping, which confirms the high phase purity of the samples and suggests that Co^{2+} ions substitute Zn^{2+} ions at the lattice sites rather than occupying interstitial positions [25]. The sharp and narrow diffraction peaks reflect the crystalline nature of the synthesized nanoparticles. The substitution of Zn^{2+} ions (ionic radius = 0.60 ˚A) by Co^{2+} ions (ionic radius = 0.58 ˚A) induces crystal defects due to the difference in ionic radii, leading to a reduction in crystallinity, an increase in lattice parameters, and an increase in unit cell volume. The changes observed in peak intensity and full width at half maximum (FWHM) can be attributed to increases in crystallite size and the presence of micro-strain within the crystal structure.

The relation

$$\frac{1}{d_{hkl}^2} = \frac{4}{3}\frac{h^2+hk+k^2}{a^2} + \frac{l^2}{c^2} \tag{1}$$

can be used to determine the spacing between planes d in a hexagonal construction. Here, a and c are lattice constants, and d_{hkl} is the interplanar distance that corresponds to its Miller indices of the h, k, and l planes.

This formula is used to get the lattice constant a for the (100) plane:

$$a = \frac{\lambda}{\sqrt{3}\sin\theta_{100}}. \tag{2}$$

For the (002) plane, the lattice constant c is computed using the formula: The lattice constant c for the (002) plane is calculated by,

$$C = \frac{\lambda}{\sin\theta_{002}} \tag{3}$$

Strain, ionic radii, crystal structure flaws, and dopant concentration all affect the lattice parameters. Additionally, the substitution of Co in the ZnO lattice is confirmed by the changes in the d-value, cell characteristics, volume, bond length, average crystallite size, shift in peak position, and peak intensity. Co doping has no effect on ZnO's hexagonal wurtzite structure.

The relationship that determines a unit cell's volume is:

$$V = \frac{\sqrt{3}}{2}a^2c \tag{4}$$

Lattice parameters are a and c. As the amount of Co doping grows, as seen in Table 1, the unit cell's volume (v) also increases. Vegard's law states that changes in the lattice constant, a rise in the unit cell's volume, and the reduced ionic radius of the Co ion relative to Zn ions [26] are indicators of the incorporation of Co^{2+} ions into the ZnO lattice. According to [27], the tetrahedral coordination of Zn^{2+} is not entirely filled by Co^{2+}. Co^{2+} in octahedral coordination with low spin r = 0.065 nm and high spin 0.075 nm [28].

The Debye-Scherrer equation:

$$D = \frac{K\lambda}{\beta\cos\theta} \tag{5}$$

was used to determine the crystalline size, where λ is the X-ray wavelength (1.5406˚A), β is the full width at half maximum (FWHM) in radians of the X-ray diffraction peak, θ is the Bragg's angle, and D is the mean size of crystallites (nm).

Table 1 lists all of the estimated lattice parameters (a and c), interplanar spacing (d), crystallite size (D) including the average crystallite size (D_{moy}), unit cell volume, as well as the peak positions given by 2θ, Miller indices (hkl), peak intensities, full width at half maximum (FWHM), and the calculated strain (ε) and stress (σ) values for each individual peak of ZnO samples with different doping percentages.

Table 1. Structural properties of ZnO samples with different doping percentages, listed by individual peaks

Sample	**2θ** (deg)	**(hkl)**	**Intensity** (u.a.)	**FWHM** (deg)	**D** (nm)	**Dmoy** (nm)	**d(˚A)**	**a(˚A)**	**c(˚A)**	**Strain** ε (%)	**Stress** σ (GPa)	**Volume** (˚A^3)
ZnO	31.92	(100)	1442.35	0.3988	20.7191	21.4631	2.7995	3.2325	—	-0.0077	0.0179	47.089
	34.56	(002)	3486.06	0.3676	22.6327		2.6023	—	5.2046			
	36.39	(101)	1810.56	0.3975	21.0375		—	—	—			
ZC1	31.91	(100)	1171.25	0.4108	20.1133	21.8926	2.8013	3.2344	—	0.0615	-0.1432	47.225
	34.54	(002)	535.81	0.3666	22.6932		2.6041	—	5.2082			
	36.36	(101)	860.9	0.3656	22.8711		—	—	—			
ZC3	31.80	(100)	109.05	0.4199	19.6721	25.1173	2.8093	3.2426		0.2037	-0.4748	47.522
	34.50	(002)	1299.408	0.3063	27.1578		2.6078	—	5.2156			
	36.28	(101)	170.29	0.2931	28.52		—	—	—			
ZC5	31.87	(100)	361.78	0.3752	22.0196	24.9678	2.8061	3.2395	—	0.2345	-0.5482	47.476
	34.49	(002)	228.05	0.3068	27.1128		2.6086	—	5.2172			
	36.26	(101)	246.57	0.3628	23.0410		—	—	—			

Fig. 2 displays the graphical representation of the lattice parameters a and c for the ZnO, ZC1, ZC3, and ZC5 thin films.

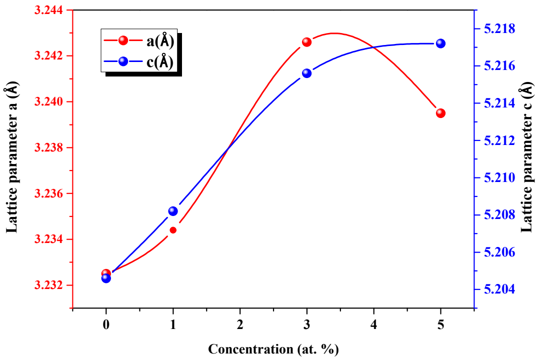

Figure 2. Variation of lattice parameters and of ZnO thin films with Co concentration

3.2. Raman Characterization

The micro-Raman spectroscopy analysis of our samples will allow us to better visualize the doping effect and also confirm the results of the X-ray diffraction study. The Raman scattering spectra of $Zn_{1-x}Co_xO$ thin films with different Cobalt contents (x = 0; 1; 3; and 5%) recorded between 50-1500 cm^{-1} are shown in Fig. 3. As shown in this figure, the Raman spectra only present:

Two predominant peaks: one at 560-570 cm^{-1} and the other peak at about 1100 cm^{-1} corresponding to the two longitudinal optical modes A_1(LO) and A_1(2LO) in all samples (pure and doped). The presence of a Raman E_2 High peak near 431 cm^{-1} (infinitely small, whose intensity decreases with doping) reveals the generation of new defects during doping following the substitution of zinc sites by cobalt ions (The ionic radius of Co^{2+} is slightly smaller than that of Zn^{2+}). In other words, the ionic radius of Co^{2+} is about 0.58 Å (0.058 nm) while that of Zn^{2+} is about 0.60 Å (0.060 nm).) [29], which confirms the DRX results that have been discussed previously. A peak at 800 cm^{-1} emitted by the glass substrate, due to good transmittance in the visible [30].

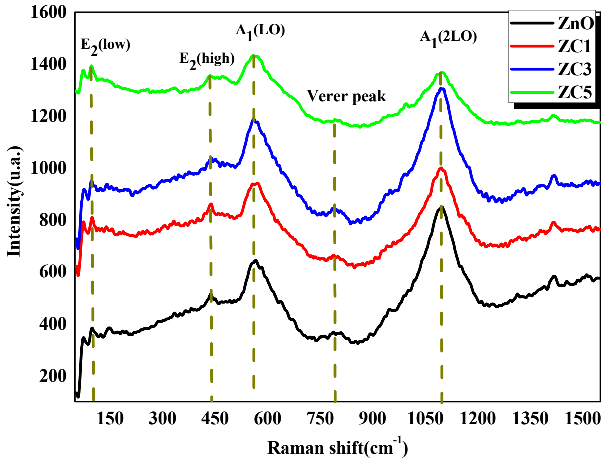

Figure 3. Micro Raman spectra for undoped and Co doped ZnO thin films

A significant perturbation of the intensities of the two predominant peaks is also observed depending on the doping element content. Electron-phonon coupling is very important to explain the optoelectronic properties of crystalline semiconductors and to translate the appearance of these two longitudinal modes A_1(LO) and A_1(2LO) as well as their intensities. This coupling strength between electrons and longitudinal phonons (LO) in polar semiconductors is determined by the intensity ratio (A_1(2LO)/A_1(LO)), between the second and first order Raman vibration of the longitudinal A1 mode [31].

Two contributing mechanisms can explain this phenomenon:

1. The long-range interaction present inside the nanocrystal, mainly due to the macroscopic electric field linked to longitudinal phonons (LO) and called the "Fröhlich mechanism". It strongly expresses the polarity of the semiconductor which serves to increase the electron-phonon coupling and implicitly the size of the crystallites [32].

2. The deformation potential which is a mechanism that relates the change in the energy of the electronic distribution to the stress in the solid, it is then sensitive to external surface defects (lattice deformation) [33] which serves to compensate for the large drop in the Fröhlich mechanism in the deformed solid, by increasing the electron-phonon coupling for infinitely small crystallite sizes. The characteristics of the A1(LO) and A1(2LO) modes are calculated and grouped in Table.2.

Table 2. Frequencies of different vibration modes of pure and doped ZnO films

Doping (% Co)	A_1 (LO)		A_1 (2LO)		$I_{A1(2LO)}/I_{A1(LO)}$
	Center (cm^{-1})	Intensity (u.a)	Center (cm^{-1})	Intensity (u.a)	
0	567.76	637.18	1099.93	851.47	1.33
1	569.64	936.42	1096.17	998.06	1.06
3	566.19	1186.23	1098.056	1300.50	1.09
5	560.55	1433.81	1094.29	1371.27	0.95

It is observed that the deformation of pure ZnO (σ = 0.0179 GPa, see Table. 1) results in a ratio of the IA_1(2LO)/IA_1(LO) intensities of 1.33. This is an important value to express the electron-phonon coupling and then shows a large polarity of the produced layers, which was translated by a large preferential orientation of the crystallites along the (002) direction as already shown in the DRX diffractograms. As the doping level increases (at 5% Co), the lattice deformation, accompanied by a slight increase in crystallite size, is the origin of the decrease in the electron-phonon coupling (from 1.33 to 0.95), while the small perturbation of the electron-phonon coupling value (from 1.06 to 1.09) is the cause of a slight improvement of the Fröhlich mechanism for the 3% Co doped ZnO layers. Beyond this dopant amount, the electron-phonon coupling value will decrease rapidly to reach 0.95. This can be explained by the quantum confinement effect governed by the strain potential and caused by the migration of cobalt (Co^{2+}) ions towards the grain boundaries. This has the effect of limiting the substitution of Zn^{2+} sites by Co^{2+} ions in the ZnO lattice as previously suggested.

3.3. Morphological Characterization

The surface condition of a sample is a very important factor in understanding certain properties such as morphology, roughness, and grain size. It is in this context that we used scanning electron microscopy (SEM) and atomic force microscopy (AFM).

3.3.1. Scanning Electron Microscopy

Fig. 4 shows SEM images taken on pure and Co-doped ZnO samples (1%, 3%, and 5%). These images show granular surface morphologies, and a non-homogeneous surface pattern is visible on all samples.

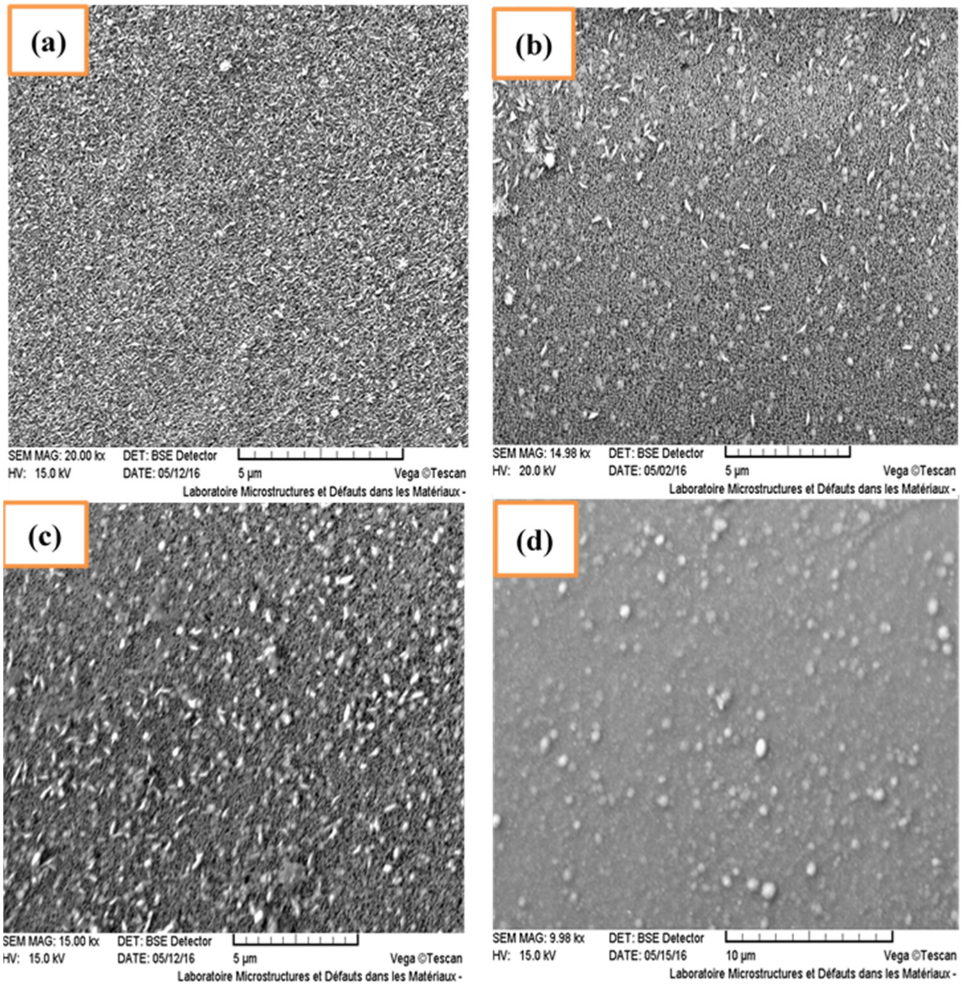

Figure 4. SEM images of the ZnO thin films at different Co doping concentrations (a): 0%, (b): 1%, (c): 3%, and (d): 5% Co

It is plausible that the smooth nature of the glass substrate hinders the perfect development of ZnO thin films. In addition, some holes, due to hydrogen bubbles released on the surface of the deposits, are observed; thus inhibiting the rate of deposition of the alloy in certain surface sites, which leads to the appearance of holes observed in the images. It is clear that they are distributed over the entire substrate for the pure ZnO sample. But for the 1% Co (Fig.4.a) doped layer, these microstructures are developed, their average diameter has increased and their density has decreased and we also notice the presence of very small particles, of clear contrast, on the surface of the grains. For the 3% Co doped layer, these bright spherical particles, more numerous than in the 1% Co doped layer. These particles are less adherent to the substrate, but have an average diameter which tends to increase. The last sample in Fig.4.c (5% Co doped layer) prepared shows good adhesion to the substrate and good coalescence of bright spherical particles. The formation of such structures in thin films obtained by spray pyrolysis is due to the relaxation of stresses resulting from the conditions of elaboration, namely: the nature of the substrate [34], the concentration of the solution [35], the nature of the solvent [36], the temperature as well as the heating rate, the drying process [37, 38] and the thickness of the layers [39, 40]. Two contributing causes are at the origin of these instabilities:

1. The desorption of the hydroxyl group containing in the solvent during annealing of the ZnO layer causes a deformation of the sample involved [41]. Consequently, a network consisting of mixed phases of liquid and solid has been constructed. Doping effect (Co) on the properties of ZnO thin films As the thermal expansion coefficients of the glass and the deposited layer are approximately equal, the annealing process does not generate any compressive stress so the grain size does not change. This explanation remains useless in our case, as our samples are produced under the same conditions and using the same protocol.

2. The second explanation is related to the internal deposition stress. When this stress exceeds a certain limit value, the flat surface becomes unstable and the average grain diameter changes. This assumption is more favorable in our case, given that our samples are produced in the same way, except for the dopant percentage that changes. As a result, spherical grains form on the surface of the thin films during production due to the cobalt doping effect.

3.3.2. Atomic force microscopy (AFM) characterization

To clearly visualize the doping effect on the topology of the obtained layers, a series of AFM images is presented in Fig.5.

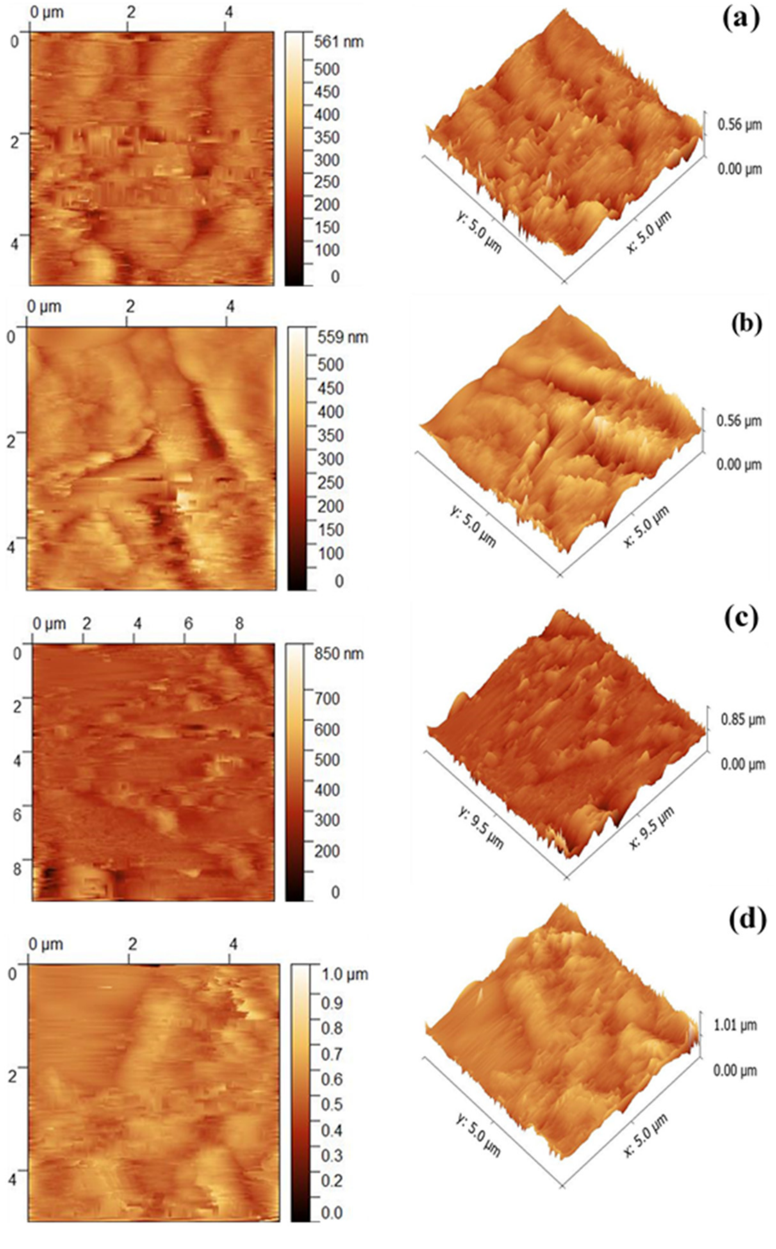

Figure 5. AFM images of the ZnO thin films at different Co doping concentrations (a) : 0%, (b): 1%, (c): 3%, and (d): 5% Co

The roughness values of the produced surfaces were estimated from the RMS (Root-Mean-Square) values. The images show the particular wrinkling structure. As these images represent the topology of the pure and doped (1% to 5% Co) ZnO layers, we note that our layers are very preferentially oriented. As observed in Fig. 5 (a, 2D and 3D), the surface of the pure ZnO layers consists of grains distributed in a mixed wavy structure, containing valleys and ridges, with an

RMS value of 37.26 nm. When the cobalt (Co) doping rate increases and reaches 1% Co, the morphology of the formed surface changes abruptly into a coalescent structure of folds (wrinkles) (Fig.5 b, 2D and 3D), probably due to the effects of internal stresses. This phenomenon can be explained by the substitution of Zn^{2+} ions by Co^{2+} ions at the deposition surface. This substitution is the origin of a compressive stress caused by the difference in the ionic radii of the two ions (Co^{2+} and Zn^{2+}). For a concentration of 3% (Fig. 5.c, 2D and 3D), the peaks become free of all types of constraints and this transformation can be due to the decrease in internal stress as previously shown in the XRD section. A good, homogeneous, and highly adherent wavy layer forms. The grains were forced to orient themselves along the (002) axis by the effect of large dipolar interactions, but when the doping value 5% Co (Fig.5 d, 2D and 3D) corresponding to the cobalt substitution limit in the ZnO matrix, the (Co^{2+}) ions tend to move towards the grain boundaries, which results in a retardation of grain growth along the c axis. Under these conditions, stress relaxation has been induced and valleys and peaks begin to disappear [42]. In addition, some holes, due to hydrogen bubbles released on the surface of the deposits, are observed; thereby inhibiting the deposition rate of the alloy in some surface sites, which leads to the appearance of holes observed on the images. To clarify this explanation more, we drew the graph that represents the crystallite size and RMN roughness deduced from AFM as a function of the % cobalt concentration in Fig. 6.

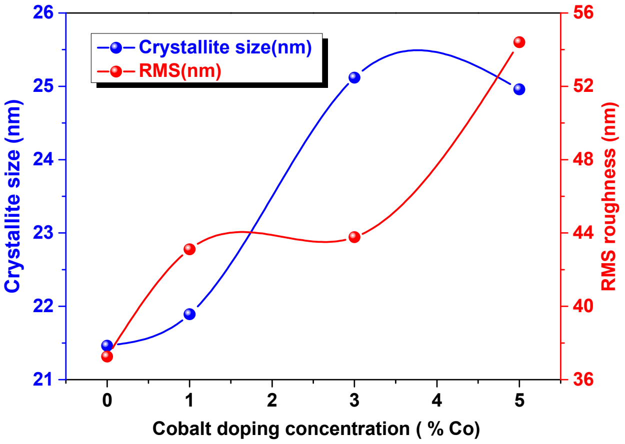

Figure 6. Crystallite size and RMN roughness deduced from AFM as a function of the % cobalt doping concentrations

3.4. Optical properties

3.4.1. UV-Visible Spectroscopy

Fig. 7 shows the optical transmission spectra of thin films of ZnO, ZC1, ZC3 and ZC5, deposited on glass substrates at 450 °C. The measurements were carried out over a wavelength range of 300–800 nm. The results indicate oscillations in all the doped films (ZC1, ZC2 and ZC3). These oscillations result from the interference between the light reflected from the film surface and the interface between the film and the substrate [43]. These oscillations were recorded by Shakit et al [44] and Aboud et al. [45]. After doping, the pure, transparent film turns green. It is evident that the transmission decreases with increasing Co concentration in the deposited films. This decrease could be attributed to the increase in the absorption of the film after doping, resulting from the contribution of Co^{2+} to the absorption process. Three absorption bands are represented in the transmission spectra at 546 nm, 598 nm and 636 nm, related to the d-d transitions of Co^{2+} ions. According to the literatures [46,47] these absorptions result from d-d transitions of high-spin Co^{2+} ions , which could be attributed to the $^4A_2 \rightarrow {}^2E(G)$, $^4A_2 \rightarrow {}^4T_1(P)$ and $^4A_2 \rightarrow {}^2A_1(G)$ transitions, respectively [47–50]. This result indicates the successful substitution of Co^{2+} into Zn^{2+} sites, where no CoO or Co_3O_4 phase was indicated by XRD results.

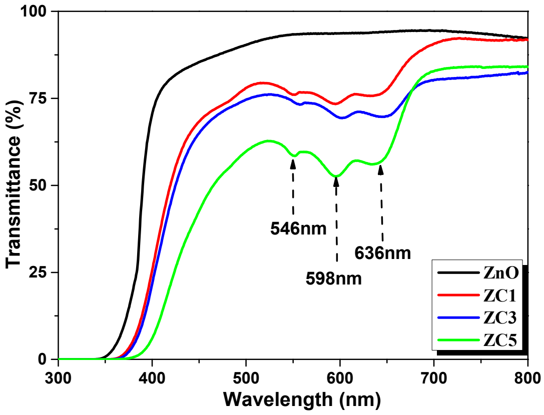

Figure 7. Optical Transmittance spectra of pure ZnO and Co doped ZnO thin films

3.4.2. Calculation of the optical gap

According to the Ridley model [51], based on the absorption band threshold, the gap energy values are estimated from the position of the predominant peak. Fig. 8 shows the first derivatives of the optical transmission as a function of the photon energy (hυ): (dT/dE). It can be seen that the band gap values decreased progressively with increasing cobalt doping concentration, with values of 3.21 eV for ZnO, 3.06 eV for ZC1, 3.01 eV for ZC3 and 2.95 eV for ZC5. However, these values are lower than those of bulk ZnO (3.27 eV). In our case, the deformation of the crystal lattice, the modification of the electronic structure, slight increase in the average grain size are mainly the origins of a decrease in the optical gap value [52]. This broadening is a direct consequence of quantum mechanics: electronic levels are confined in a potential well whose size is close to the typical wavelengths of electrons. By sufficiently increasing the size of semiconductor particles, the absorption threshold is shifted towards lower energies, the gap becomes wider and the electronic structure is affected [53].

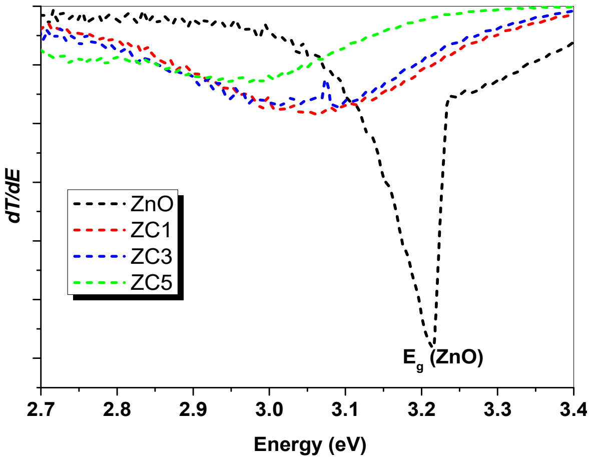

Figure 8. The first derivative of transmittance (dT/dE) as a function of energy (hν) for ZnO, ZC1, ZC3, and ZC5 thin films

The Urbach energy is a characteristic parameter of energetic disorder in the band edges. It was calculated based on the following equation:

$$\ln(\alpha) = \ln(\alpha_0) + \frac{h\upsilon}{E_U} \tag{6}$$

where α_0 is a constant, hν is the photon energy, and E_U is the Urbach energy.

The results of the band gap and Urbach energy calculations are represented in Fig. 9. The Urbach energy was found to increase with increasing Co content, indicating a rise in the energetic disorder within the films, which is directly related to structural defects. This result correlates well with the increase in the intensity of the A1(low)/E1(low) peaks as a function of Co doping, as observed in the Raman spectra.

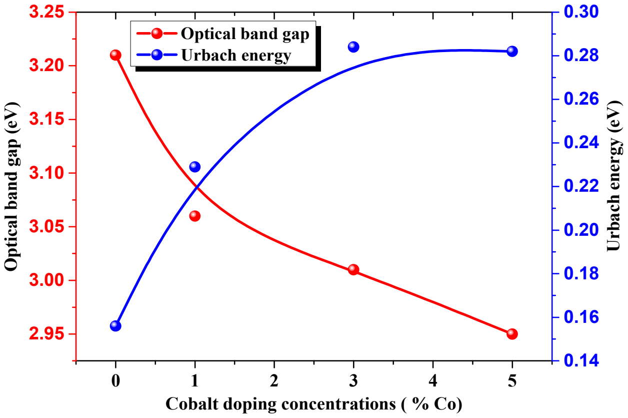

Figure 9. The evolution of both the optical gap energy (Eg), the Urbach energy (Eu) as a function of Co doping

3.5. Magnetic properties

Cobalt-doped ZnO ($Zn_{1-x}Co_xO$) thin films exhibit interesting magnetic properties, particularly in the context of diluted magnetic semiconductors (DMS). These materials are attracting attention for potential applications in spintronics, which exploits both charge and spin of electrons [54,55]. In this section, we will study the magnetic properties of (1, 3, and 5 Co) doped ZnO thin films. Fig. 10 (a,b) shows the hysteresis loops taken from the Co-doped ZnO samples (1%, 3%, and 5%) in room temperature. The magnetic parameters, namely saturation field (Hs), coercivity (H_C), saturation magnetization and remanent magnetization (MR), estimated from the M-H curves at room temperature, are presented in Table 3.

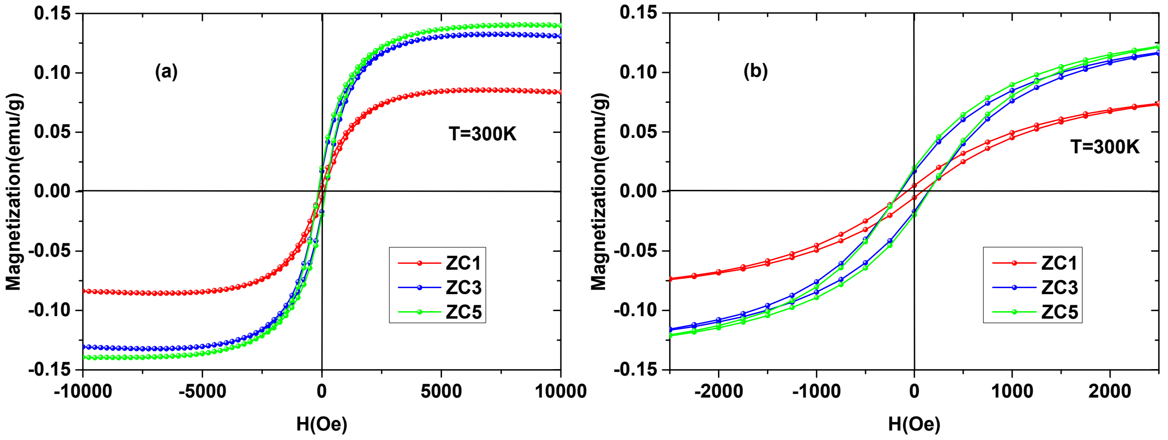

Figure 10. hysteresis loops taken from the Co-doped ZnO samples (1%, 3%, and 5%) in room temperature

Table 3. Values of different magnetic properties

Doping (% Co)	Saturation field (Hs)	Coercive field (Hc)	Saturation magnetization Ms	Remanence Mr
1	7000	78.92	0.08543	0.00511
3	7500	143.82	0.13242	0.01702
5	8250	151.45	0.14033	0.01983

The curves show a hysteresis or remanence indicating the presence of ferromagnetism but at a concentration of 1% Cobalt and present a weak ferromagnetism. Moreover, the saturation field Hs is increased with increasing cobalt concentration (Fig.8, a)) and the low field region of hysteresis loops (Fig. 8(b)) shows that the coercive field Hc values are in the range of 78.92 to 151.45 Oe. Studies [56-58] show that cobalt-doped ZnO can exhibit ferromagnetism at room temperature, which is of interest for spintronics, but the origin of this ferromagnetism is still controversial this behavior depends on several experimental factors are:

- Co concentration: Low doping (<5%) sometimes promotes ferromagnetism, but at higher concentrations, the behavior often becomes paramagnetic or antiferromagnetic.
- Presence of free carriers (electrons): Ferromagnetism can be induced by the presence of free carriers (Zener model), and the presence of oxygen vacancies can promote it.
- The Synthesis method strongly influences magnetic properties. Ferromagnetism is sometimes observed in inhomogeneous thin films. This ferromagnetic signal was observed by Mamani et al. [59] on thin films of cobalt-doped ZnO prepared by EB-PVD at room temperature and on thin films of Co and N doped ZnO prepared by two distinct methods Sol-gel and PLD by Ramasubramanian et al. [60] and by Dhruvashi et al [61].

These results, however, seem to contradict the ferromagnetic character of thin films produced by magnetron sputtering [62,63] and by other production methods [64-68]. The origin of this inconsistency is still not clear, but there are hypotheses according to which ferromagnetism would be sensitive to the methods and conditions of production of Co doped ZnO [69].

5. CONCLUSION

In this work, we conducted a study focused on zinc oxide in the form of cobalt-doped thin films, with the objective of developing and then investigating the doping effect on the structural, morphological, optical, and magnetic properties of ZnO thin films developed by spray technique. This configuration is the ultimate key to the potential applications of $Zn_xCo_{1-x}O$ thin films. This is why we fabricated a series of samples by varying the doping level. To fully understand the impact of this factor on the properties of ZnO, we used a range of characterization techniques, including X-ray diffraction, Raman spectrophotometry, scanning electron microscopy (SEM), atomic force microscopy (AFM), UV-visible spectrophotometry, and spectroscopy, and vibrating sample magnetometer (VSM).

Structural XRD studies of the films reveal that our films are polycrystalline with a hexagonal wurtzite structure and a preferential unidirectional orientation, along the [002] direction. XRD analysis clearly indicates that the dopant is incorporated into the ZnO lattice without any phase segregation occurring in these films. Raman spectroscopic analyses demonstrated the very good texturization of the films, by the presence of two intense, dominant peaks corresponding to the longitudinal A_1(LO) and its 2nd order A_1(2LO) vibration modes. SEM images reveal granular surface morphologies, their densities and diameters increasing with increasing doping levels, and a non-homogeneous surface pattern is visible on all samples. However, the AFM images confirmed the XRD results, showing a vertical and preferential growth of the grains along the (002) direction, and also that the layers consist of grains distributed in a mixed wavy structure, containing valleys and ridges, with an RMS value between 37.25 nm and 54.4 nm. The optical characterization of the developed layers revealed oscillations in all the doped films. These oscillations result from the interference between the light reflected by the film surface and the interface between the film and the substrate. It is evident that the transmission decreases with the increase in Co concentration in the deposited films. This decrease is attributed to the increase in the absorption of the film after doping, resulting from the contribution of Co^{2+} to the absorption process. This result indicates the successful substitution of Co^{2+} in the Zn^{2+} sites. The doping effect on the gap energy of ZnO films is manifested by a decrease (from 3.212 eV to 2.95 eV) as a function of the dopant concentration, which may be due to quantum confinement in the ZnO matrix. The VSM revealed that all films are intrinsically ferromagnetic. The substantial enhancement of ferromagnetism has been observed upon increase Co doping. Hence the effect of Co doping on ZnO thin films is highly enhanced ferromagnetism and proper Co substituted ZnO films. Overall, these results demonstrate that cobalt doping significantly affects the physical properties of ZnO, offering the potential to tailor them for future electronic or optoelectronic applications.

Finally, due to the vast complexity of the effect of cobalt doping on the ferromagnetic properties of the ZnO thin films, several issues are still open for future investigation in order to fully understand the abilities and limitations of influence cobalt doping on the ferromagnetic properties of the ZnO thin films. Hopefully, the results presented in this work gives a contribution to this understanding

ORCID

Abderrahmane Bouabellou, https://orcid.org/0009-0009-0854-9616
Djamel Belfennache, https://orcid.org/0000-0002-4908-6058

REFERENCE

[1] M. Vali, and A. Bayani, Mat Sci Semicon Proc. **195**, 109599 (2025). https://doi.org/10.1016/j.mssp.2025.109599
[2] Y. Sun, T. Wang, J. Luo, J. Chen, W. Huang, and J. Ding, Mater. Today Electron. **12**, 100151 (2025). https://doi.org/10.1016/j.mtelec.2025.100151
[3] D. Belfennache, D. Madi, N. Brihi, M.S. Aida, and M.A. Saeed, Appl. Phys. A, **124**, 697 (2018). https://doi.org/10.1007/s00339-018-2118-z
[4] I. Hanif, and I. Iatsunskyi, Int. J. Hydrog. Energy, **109**, 174 (2025). https://doi.org/10.1016/j.ijhydene.2025.01.491
[5] R. Ouldamer, D. Belfennache, D. Madi, R. Yekhlef, S. Zaiou, and M.A. Ali, J. Ovonic. Res. **20**(1), 45 (2024). https://doi.org/10.15251/JOR.2024.201.45
[6] Y. Benkrima, S. Benhamida, and D. Belfennache, Dig. J. Nanomater. Bios. **18**(1), 11 (2023) https://doi.org/10.15251/DJNB.2023.181.11
[7] Y. Benkrima, M.E. Soudani, D. Belfennache, H. Bouguettaia, and A. Souigat, J. Ovonic. Res. **18**(6), 797 (2022). https://doi.org/10.15251/JOR.2022.186.797
[8] Ü. Özgür, Ya. I. Alivov, C. Liu, A. Teke, M.A. Reshchikov, S. Doğan, V. Avrutin, *et al.*, J. Appl. Phys. **98**(4), 041301 https://doi.org/10.1063/1.1992666
[9] R. Kurniawan, I.M. Sutjahja, T. Winata, T. S. Herng, J. Ding, A. Rusydi, and Y. Darma, Opt. Mater. Express, **7**(11), 3902 (2017). https://doi.org/10.1364/OME.7.003902
[10] L. Wang, Comput. Methods Appl. Mech. Eng. **445**, 118205 (2025). https://doi.org/10.1016/j.cma.2025.118205
[11] Z. Wang, Q. Chen, Z. Qi, Z. Song, Z. Wang, B. Cao, S. Pan, J. Pang, and W. Wang, Intermetallics, **185**, 108886 (2025). https://doi.org/10.1016/j.intermet.2025.108886
[12] D. Belfennache, N. Brihi, and D. Madi, Proceeding of the IEEE xplore, 8th (ICMIC) (2016). 7804164, 497–502 (2017). https://doi.org/10.1109/ICMIC.2016.7804164
[13] Y. Benkrima, D. Belfennache, R. Yekhlef, and A. M. Ghaleb, Chalcogenide Lett. **20(8)**, 609-618 (2023). https://doi.org/10.15251/CL.2023.208.609
[14] M. Shkir, Mater. Sci. Eng. B, **284**, 115861 (2022). https://doi.org/10.1016/j.mseb.2022.115861
[15] S.D. Lokhande, H.A. Varudkar, M.B. Awale, L.H. Kathwate, J.S. Dargad, and V.D. Mote, Materials Letters, **337**, 133919 (2023). https://doi.org/10.1016/j.matlet.2023.133919
[16] F. Hadji, Y. Rassim, D. Belfennache, R. Yekhlef, N. Bounar, M.A. Bradai, M. Hemdan, and M.A Ali, Egypt. J. Chem. **68,** 63 (2025). https://doi.org/10.21608/ejchem.2024.283147.9600
[17] O.A. Akinwumi, K.O. Olumurewa, A.T. Famojuro, and O.O. Akinwunmi, Next Materials, **8**, 100883 (2025). https://doi.org/10.1016/j.nxmate.2025.100883
[18] S. Mahdid, D. Belfennache , D. Madi, M. Samah, R. Yekhlef, and Y. Benkrima,. J. Ovonic. Res. **19(5)**, 535-545 (2023). https://doi.org/10.15251/JOR.2023.195.535.
[19] R. Ouldamer, D. Madi, and D. Belfennache, in: *Advanced Computational Techniques for Renewable Energy Systems, IC-AIRES, 2022*, Lecture Notes in Networks and Systems, **591**, edited by M. Hatti, (Springer, Cham. 2023). pp. 700-705. https://doi.org/10.1007/978-3-031-21216-1_71
[20] F. Saker, L. Remache, D. Belfennache, K.R. Chebouki, and R. Yekhlef, Chalcogenide Letters, **22**(2), 151 (2025). https://doi.org/10.15251/CL.2025.222.151
[21] R.C. Greenhalgh, A. Abbas, V. Kornienko, and J.M. Walls, Sol. Energy Mater. Sol. Cells, **292**, 113742 (2025). https://doi.org/10.1016/j.solmat.2025.113742
[22] Y. Bellal, A. Bouhank, D. Belfennache, R. Yekhlef, East Eur. J. Phys, (**1**), 170-176 (2025). https://doi.org/10.26565/2312-4334-2025-1-16
[23] N.K. Singh, V. Koutu, and M.M. Malik, J. Sol-Gel Sci. Technol. **91**, 324 (2019). https://doi.org/10.1007/s10971-019-05004-4

[24] I. Djerdj, Z. Jagliˇci´c, D. Arˇcon, and M. Niederberger, Nano scale, **2**(7), 1096 (2010). https://doi.org/10.1039/c0nr00148a
[25] U. Godavarti, V.D. Mote, and M. Dasari, J. Asian Ceram. Soc. **5**, 391 (2017). https://doi.org/10.1016/j.jascer.2017.08.002
[26] L. Vegard, Zeitschrift für Physik, **5**(1), 17 (1921). http://dx.doi.org/10.1007/BF01349680
[27] S. Roguai, and A. Djelloul, Appl. Phys. A: Mater. Sci. Process. **125**(12), 1 (2019). https://doi.org/10.1007/s00339-019-3118-3
[28] M. Bouloudenine, N. Viart, S. Colis, J. Kortus, and A. Dinia, Appl. Phys. Lett. **87**, 05250 (2005). https://doi.org/10.1063/1.2001739
[29] A. Manikandan, E. Manikandan, B. Meenatchi, S. Vadivel, S.K. Jaganathan, R. Ladchumananandasivam, M. Henini, *et al.*, J. Alloys Compd. **723,** 1155 (2017). https://doi.org/10.1016/j.jallcom.2017.06.336
[30] I.S. Yahia, A.A.M. Farag, M. Cavas, and M.F. Yakuphanoglu, Superlattices Microstruct. **53**, 63 (2013). https://doi.org/10.1016/j.spmi.2012.09.008
[31] A.C. Gandhi, W.S. Yeoh, M.A. Wu, C.H. Liao, D.Y. Chiu, W.L. Yeh, and Y.L., Huang, Nanomaterials, **8**(8), 632 (2018). https://doi.org/10.3390/nano8080632
[32] G. Scamarcio, V. Spagnolo, G. Ventruti, M. Lugara, and M.G.C. Righini, Phys. Rev. B, **53**, R10489 (1996). https://doi.org/10.1103/PhysRevB.53.R10489
[33] A.K. Ojha, M. Srivastava, S. Kumar, R. Hassanein, J. Singh, M.K. Singh, and A. Materny, Vib. Spectrosc. **72,** 90 (2014). https://doi.org/10.1016/j.vibspec.2014.02.013
[34] W. Chebil, Indian Journal of Pure & Applied Physics, (IJPAP), **53**(8), 521-529 (2015).
[35] M. Soylu, and M. Coskun, J. Alloys. Compd. **741**, 957 (2018). https://doi.org/10.1016/j.jallcom.2018.01.079
[36] C.Y. Tsay, K.S. Fan, Y.W. Wang, C.J. Chang, Y.K. Tseng, and C.K. Lin, Ceramics International, **36**(6), 1791 (2010). https://doi.org/10.1016/j.ceramint.2010.03.005
[37] J. Li, D. Yang, and X. Zhu, Materials technology, **33**(3), 198 (2018). https://doi.org/10.1080/10667857.2017.1396775
[38] C.Y. Tsay, K.S. Fan, S.H. Chen, and C.H. Tsai, J. Alloys. Compds. **495**(1), 126 (2010). https://doi.org/10.1016/j.jallcom.2010.01.100
[39] J. Li, X. Zhu, P. Gu, X, Zhang, X. Li, Y. Chen, and D. Yang, Materials Technology, **34**(2), 80 (2018). https://doi.org/10.1080/10667857.2018.1523086
[40] N. Kaneva, A. Bojinova, K. Papazova, D. Dimitrov, I. Svinyarov, and M. Bogdanov, Bulg. Chem. Commun. **47**, 395 (2015).
[41] M. Yilmaz, and A. Şakir, Mater. Sci. Semicond. Process, **40**, 162 (2015). https://doi.org/10.1016/j.mssp.2015.06.064
[42] A. Maache, A.Chergui, D. Djouadi, B. Benhaoua, A. Chelouche, and M. Boudissa, Optik, **180**, 1018 (2019). https://doi.org/10.1016/j.ijleo.2018.11.002
[43] J. Singh, *Optical Properties of Condensed Matter and Applications*, vol. 6, (John Wiley & Sons, 2006). https://doi.org/10.1002/0470021942
[44] N. Shakti, and P.S. Gupta, Appl. Phys. Res. **2**(1), 19 (2010) https://doi.org/10.5539/apr.v2n1p19
[45] A.A. Aboud, M. Shaban, and N. Revaprasadu, RSC Adv. **9**(14), 7729 (2019). https://doi.org/10.1039/c8ra10599e
[46] S. Yang, B.Y. Man, M. Liu, C.S. Chen, X.G. Gao, C.C. Wang, and B. Hu, Phys. B: Condens. Matter, **405**(18), 4027 (2010). https://doi.org/10.1016/j.physb.2010.06.050
[47] C. Song, F. Zeng, K.W. Geng, X.B. Wang, Y.X. Shen, and F. Pan, J. Magn. Magn Mater. **309**(1), 25 (2007). https://doi.org/10.1016/j.jmmm.2006.06.012
[48] E. Gungor, T. Gungor, D. Caliskan, A. Ceylan, and E. Ozbay, Appl. Surf. Sci. **318**, 309 (2014). https://doi.org/10.1016/j.apsusc.2014.06.132
[49] M. Ivill, S.J. Pearton, S. Rawal, L. Leu, P. Sadik, R. Das, A.F. Hebard, *et al.*, New J. Phys. **10**(6), 065002 (2008). https://doi.org/10.1088/1367-2630/10/6/065002
[50] A.C. Tuan, *et al.*, Phys. Rev. B, **70**, 054424 (2004). https://doi.org/10.1103/PhysRevB.70.054424
[51] B.K. Ridley, *Quantum Processes in Semiconductors*, 5th edn. (Oxford, 2013). https://doi.org/10.1093/acprof:oso/9780199677214.001.0001
[52] S.H. Deng, M.Y. Duan, M. Xu, and L. He, Physica B: Condensed Matter, **406**(11), 2314 (2011). https://doi.org/10.1016/j.physb.2011.03.067
[53] A. Salah, A.M. Saad, and A.A. Aboud, Optical Materials, **113**, 110812 (2021). https://doi.org/10.1016/j.optmat.2021.110812
[54] A.T. Naziba, M.T. Nafisa, R. Sultana, Md.F. Ehsan, A.R.M. Tareq, R. Rashid, H. Das, *et al.*, J. Magn. Magn. Mater, **593**, 171836 (2024). https://doi.org/10.1016/j.jmmm.2024.171836
[55] R.A. Torquato, S.E. Shirsath, R.H.G.A. Kiminami, and A.C.F.M. Costa, Ceramics International, **44**(4), 4126 (2018). https://doi.org/10.1016/j.ceramint.2017.11.213
[56] M. Zhong, W. Wu, H. Wu, and S. Guo, J. Alloys. Compds, **765**, 69 (2018). https://doi.org/10.1016/j.jallcom.2018.06.228
[57] J.K. Park, K.W. Lee, S.J. Noh, H.S. Kim, and C.E. Lee, Curr. Appl. Phys. **14**(2), 206 (2014). https://doi.org/10.1016/j.cap.2013.11.004
[58] B. Salameh, A.M. Alsmadi, and M. Shatnawi, J. Alloys. Compds. **835**, 155287 (2020). https://doi.org/10.1016/j.jallcom.2020.155287
[59] N.C. Mamani, J. Alloys. Compds**. 695**, 2682 (2017). https://doi.org/10.1016/j.jallcom.2016.11.183
[60] S. Ramasubramanian, R. Thangavel, M. Rajagopalan, A. Thamizhavel, K. Asokan, D. Kanjilal, and J. Kumar, Curr. Appl. Phys. **13**, 1547 (2013). https://doi.org/10.1016/j.cap.2013.05.010
[61] Dhruvashi, and P.K. Shishodia, Thin Solid Films, **612**, 55 (2016). https://doi.org/10.1016/j.tsf.2016.05.028
[62] X.J. Liu, C. Song, P.Y. Yang, F. Zeng, and F. Pan, Appl. Surf. Sci. **254**, 3167 (2008). https://doi.org/10.1016/j.apsusc.2007.10.078
[63] W. Zhuliang, L. Xiaoli, J. Fengxian, T. Baoqiang, L. Baohua, and X. Xiaohong, Rare. Metal. Mat. Eng. **37**(5), 0831 (2008). https://doi.org/10.1016/S1875-5372(09)60021-7
[64] H.-J. Lee, S.-Y. Jeong, C. Cho, and C. Park, Appl. Phys. Lett. **81**, 4020 (2002). https://doi.org/10.1063/1.1517405
[65] C.B. Fitzgerald, M. Venkatesan, J.G. Lunney, L.S. Dorneles, and J.M.D. Coey, Appl. Surf. Sci. **247**, 493 (2005). https://doi.org/10.1016/j.apsusc.2005.01.043

[66] L.S. Dorneles, M. Venkatesan, R. Gunning, P. Stamenov, J. Alaria, M. Rooney, J.G. Lunney, and J.M.D. Coey, J. Magn. Magn. Mater. **310**, 2087 (2007). https://doi.org/10.1016/j.jmmm.2006.10.1017

[67] A. Zukova, A. Teiserskis, V. Kazlauskiene, Y.K. Gun'ko, and S. Dijken, J. Magn. Magn. Mater. **316**, e203 (2007). https://doi.org/10.1016/j.jmmm.2007.02.090

[68] J.H. Kim, H. Kim, D. Kim, Y.E. Ihm, and W.K. Choo, J. App. Phys. **92**, 6066 (2002). https://doi.org/10.1063/1.1513890

[69] R.K. Singhal, A. Samariya, Y.T. Xing, S. Kumar, S.N. Dolia, U.P. Deshpande, T. Shripathi, and E.B. Saitovitch, J. Alloys. Compd. **496**, 324 (2010). https://doi.org/10.1016/j.jallcom.2010.02.005

ВПЛИВ ЛЕГУВАННЯ КОБАЛЬТОМ НА СТРУКТУРНІ, МОРФОЛОГІЧНІ, ОПТИЧНІ ТА МАГНІТНІ ВЛАСТИВОСТІ ТОНКИХ ПЛІВОК ZnO, ВИГОТОВЛЕНИХ ТЕХНІКОЮ УЛЬТРАЗВУКОВОГО НАПИЛЕННЯ

З. Даас[a], А. Буабеллу[a], К. Даас[b], Д. Бельфеннаше[c], К. Бензуаї[a], М. Махталі[a], Р. Єхлеф[c]
[a]Лабораторія тонких плівок та інтерфейсів, Університет Костянтина 1-Фрер Ментурі, 25017 Костянтин, Алжир
[b]Лабораторія математики та їх взаємодій, Університетський центр Буссуфа Абдельхафіда, Міла, Алжир
[c]Науково-дослідний центр промислових технологій CRTI, P.O. Box 64, Черага, 16014 Алжир, Алжир

Тонкі плівки оксиду цинку-кобальту ($Zn_{1-x}Co_xO$) відносяться до напівпровідникового матеріалу на основі оксиду цинку (ZnO), легованого кобальтом (Co). Цей матеріал вивчається головним чином через його модифіковані магнітні, електронні та оптичні властивості, зокрема в контексті розбавлених магнітних напівпровідників (РМП). У цьому дослідженні аналізується вплив легування кобальтом на структурні оптичні та магнітні властивості тонких плівок ZnO, виготовлених за допомогою недорогого, масштабованого методу ультразвукового напилення. Тонкі плівки оксиду цинку-кобальту (Zn1−xCoxO) були успішно нанесені на скляні підкладки за допомогою методу ультразвукового напилення при температурі підкладки 450 ◦C, з концентраціями легування кобальтом x = 0%, 1%, 3% та 5%. Рентгенівський дифракційний (XRD) аналіз виявив гексагональну структуру вюрциту для всіх зразків без вторинних фаз, що свідчить про ефективне включення іонів Co2+ у решітку ZnO. Раманівська спектроскопія вказала на появу структурного безладу та дефектних мод, що узгоджується зі збільшенням енергії Урбаха. Скануюча електронна мікроскопія (СЕМ) показала зернисту морфологію поверхні, а на всіх зразках видно неоднорідний малюнок поверхні. Атомно-силова мікроскопія (АСМ) показала збільшення шорсткості поверхні та розміру зерен зі збільшенням концентрації легування. Оптичні вимірювання підтвердили високий коефіцієнт пропускання у видимому діапазоні та поступове зменшення ширини оптичної забороненої зони від 3,21 еВ до 2,95 еВ зі збільшенням вмісту Co. Спектроскопія та вібраційний магнітометр (VSM) показали, що всі плівки є внутрішньо феромагнітними. Було виявлено, що походження феромагнетизму є внутрішньою властивістю тонких плівок ZnO, легованих кобальтом.

Ключові слова: *техніка напилення; тонкі плівки ZnO; легування кобальтом; раманівська спектроскопія; розбавлені магнітні напівпровідники (РМН)*